

## Investigation of ground vibrations induced by trains moving on saturated transversely isotropic ground



Guangyun Gao<sup>a,b,\*</sup>, Chenxiao Xu<sup>a,b</sup>, Juan Chen<sup>a,b</sup>, Jian Song<sup>c</sup>

<sup>a</sup> Department of Geotechnical Engineering, Tongji University, Shanghai 200092, China

<sup>b</sup> Key Laboratory of Geotechnical and Underground Engineering of Ministry of Education, Tongji University, Shanghai 200092, China

<sup>c</sup> Key Laboratory of Ministry of Education for Geomechanics and Embankment Engineering, College of Civil and Transportation Engineering, Hohai University, Nanjing 210098, China

### ARTICLE INFO

#### Keywords:

Ground vibration  
Moving train loads  
Transversely isotropic saturated soil  
2.5D FEM  
Excess pore water pressure

### ABSTRACT

A 2.5D FEM (finite element method) is used to investigate the effects of soil parameters of transversely isotropic (cross anisotropic) saturated soil on ground vibrations and excess pore water pressures induced by moving train loads. The governing equations of transversely isotropic saturated soil are derived from the Boit's theory in frequency domain by applying the Fourier transform with respect to time, and 2.5D FE model is then established using Galerkin method. Correctness of the proposed model is validated with published data. Numerical results illustrate that the decrement of vibration amplitude and excess pore water pressure caused by the increment of vertical elastic modulus is more significant than that of the horizontal direction. Poisson ratios in both directions have little effect on ground vibrations, while an increase in horizontal Poisson ratio results in a significant increment in excess pore water pressure.

### 1. Introduction

Railway train has been a major mode of public transportation, especially in China. With the rapid development of high-speed railways, the environmental vibration caused by moving trains is becoming more widely concerned. Natural soils widely distributed in coastal area usually is exhibited the characteristic of cross-anisotropy or transverse isotropy due to sedimentation or consolidation. Therefore, researchers should pay more attention on the vibrations of transversely isotropic (cross anisotropic) ground.

Many experimental methods are adopted to study the property of transversely isotropic soil. For example, Kuwano et al. [1] used bender elements and trigger-accelerometers to measure elastic wave velocities transmitted vertically in triaxial specimens of sand, gravel and glass beads. Nishimura [2] adopted high-precision triaxial apparatus to study cross-anisotropic deformation characteristics of natural sedimentary clays. Other researchers studied the analytical solution of wave propagation in transversely isotropic ground. Papargyri-Beskou et al. [3] studied the wave propagation in gradient elastic solids and structures. Zymnis et al. [4] presented closed-form analytical solution for estimating far-field ground deformations caused by shallow tunneling in a linear elastic soil mass with cross-anisotropic stiffness properties. Ahmadi and Eskandari [5] analyzed the vibrations of rigid circular disk

and strip embedded in a transversely isotropic solid. Ogden and Singh [6] investigated the effect of rotation and initial stress on the propagation of waves. Recently, Ai and Ren [7] analyzed the vibration of a transversely isotropic solid subject to a moving loading using the analytical element method.

Apart from the experimental and analytical studies, numerical method is becoming a promising method in study of this problem with its feasibility for dealing with actual problems with irregular geometry. Abedrrahim [8] presented a coupling method of finite and hierarchical infinite elements to solve a non-homogeneous cross-anisotropic half-space subjected to a non-uniform circular loading. These methods showed good performance in predicting vibration in non-homogenous soils, however, such models are rather expensive in calculation time and memory space. To improve the computational efficiency and ensure the accuracy of computational model, a 2.5D FEM was used for solving the ground vibrations induced by a moving train [9–12]. The 2.5D FEM conducts Fourier transform along the train moving direction, and solves the three dimension problem with a two dimensional FE grids which is dispersed on section perpendicular to the train moving direction. It is firstly used in seismic analysis, and then employed to solve dynamic response under train loads by Yang and his collaborators [9,10]. Nevertheless, published results using 2.5 D FEM are all in homogenous or layered elastic and saturated soils, study on ground

\* Correspondence to: College of Civil Engineering, Tongji University, Shanghai 200092, China.  
E-mail address: [gaoguangyun@263.net](mailto:gaoguangyun@263.net) (G. Gao).

borne vibration under moving train loads in transversely isotropic saturated soil is not yet reported.

In view of this, based on Biot theory and the Galerkin method, this paper establishes a 2.5D FEM of transversely isotropic saturated soil together with flow viscoelastic boundary conditions, to predict ground vibrations in such soils subjected to train loads; and the effects of mechanical parameters of transversely isotropic saturated soil on the ground vibration and excess pore water pressure are studied in detail.

## 2. Equations of $u$ - $p$ format for 2.5D FEM

The finite element model is the same as that in Ref. [11], track and ground are simplified as Euler-Bernoulli beam and transversely isotropic saturated porous medium, respectively. The train moves along the track with a velocity  $c$ , the expression of train loads can be seen in Ref. [11]. The material and geometric properties are assumed to be constant along the train moving direction. Coordinates system of the finite element model is the same as that in Ref. [11], where  $x$  is the train moving direction,  $y$  is the direction perpendicular to track, and  $z$  is the vertical direction, the track center is the origin of coordinates. In addition, the height of embankment is set to be 1.0 m, and underground water level is at the ground surface.

According to Biot's theory of wave propagation in fluid-saturated porous medium, the dynamic motion equations of a fully saturated poroelastic medium can be expressed as follows [11]:

$$\sigma_{ij,j} + F_i = \rho u''_i + \rho_f W''_i \quad (1)$$

$$-\frac{n}{K_f} p' = W'_{,i,i} + u'_{,i,i} \quad (2)$$

$$-p_{,i} = \rho_f u'' + \frac{\rho_f}{n} W''_i + \frac{\rho_f g}{K_d} W'_i \quad (3)$$

in which  $\sigma_{ij}$  is the stress of porous medium and  $F_i$  is the body force of the solid skeleton;  $\rho$  and  $\rho_f$  denote the bulk density of the porous medium and the density of the pore fluid,  $\rho = \rho_s(1 - n) + n\rho_f$ , in which  $\rho_s$  is the density of the solid skeleton and  $n$  is the porosity of the porous medium;  $W_i = n(w_i - u_i)$  is the average displacement of the pore fluid relative to the solid skeleton, in which  $w_i$  and  $u_i$  denote the infiltration displacements of pore fluid and the average displacement of solid skeleton, respectively;  $p$  is the excess pore water pressure and  $g$  is the acceleration of gravity;  $K_f$  and  $K_d$  are the bulk modulus of pore fluid and the permeability of the porous medium, respectively; (') indicates differentiation with respect to time  $t$ .

The Fourier transformation of function  $u(x, y, z, t)$  with respect to  $x$ -coordinate and time  $t$  is defined by:

$$\bar{u}(\varepsilon_x, y, z, \omega) = \int_{-\infty}^{+\infty} \int_{-\infty}^{+\infty} u(x, y, z, t) e^{i\varepsilon_x x} e^{-i\omega t} dx dt \quad (4)$$

The corresponding inverse transforms with respect to  $\varepsilon_x$  and  $\omega$  is given by:

$$u(x, y, z, t) = \frac{1}{4\pi^2} \int_{-\infty}^{+\infty} \int_{-\infty}^{+\infty} \bar{u}(\varepsilon_x, y, z, \omega) e^{-i\varepsilon_x x} e^{i\omega t} d\varepsilon_x d\omega \quad (5)$$

where  $\omega$  and  $\varepsilon_x$  represent circular frequency and the horizontal wave-number corresponding to  $x$ -direction, respectively.

Based on the generalized Hooke's law, stress-strain relationship and effective stress principle of soil, the relationship between stresses and displacements of soil are given as:

$$\begin{cases} \sigma_x = C_{11} \frac{\partial u}{\partial x} + C_{12} \frac{\partial v}{\partial y} + C_{13} \frac{\partial w}{\partial z} - p & \tau_{yz} = C_{44} \left( \frac{\partial v}{\partial z} + \frac{\partial w}{\partial y} \right) \\ \sigma_y = C_{12} \frac{\partial u}{\partial x} + C_{11} \frac{\partial v}{\partial y} + C_{13} \frac{\partial w}{\partial z} - p & \tau_{zx} = C_{44} \left( \frac{\partial w}{\partial x} + \frac{\partial u}{\partial z} \right) \\ \sigma_z = C_{13} \frac{\partial u}{\partial x} + C_{13} \frac{\partial v}{\partial y} + C_{33} \frac{\partial w}{\partial z} - p & \tau_{xy} = C_{66} \left( \frac{\partial u}{\partial y} + \frac{\partial v}{\partial x} \right) \end{cases} \quad (6)$$

where  $u$ ,  $v$  and  $w$  are respectively displacements of soil skeleton in  $x$ ,  $y$  and  $z$  directions;  $C_{ij}$  ( $i, j = 1, 2, 3, 4, 6$ ) are mechanical parameters of

transversely isotropic soil, which can be expressed in horizontal and vertical elastic moduli, horizontal and vertical Poisson's ratio and the shear modulus. Elastic modulus in complex form is introduced to account for the material damping.

In order to eliminate time derivatives in Eq. (3), the Fourier transformation with respect to time is performed on Eq. (3). As a result, the equation is transformed into the frequency domain. By using the derivative nature of Fourier transform, the following equation can be obtained:

$$W_i = F(\omega^2 \rho_f \bar{u}_i - \bar{p}_i) \quad (7)$$

in which  $F = nK_d/(i\omega\rho_f gn - \omega^2 K_d \rho_f)$ , variables with a bar above indicate the components in frequency domain.

Substituting Eqs. (6) and (7) into Eq. (1), and then performing Fourier transformation with respect to time, the balance equations of mechanics parameters in frequency domain are given by:

$$\begin{cases} (C_{11} \frac{\partial^2}{\partial x^2} + C_{66} \frac{\partial^2}{\partial y^2} + C_{44} \frac{\partial^2}{\partial z^2}) \bar{u} + (C_{12} + C_{66}) \frac{\partial^2 \bar{v}}{\partial x \partial y} + \\ (C_{13} + C_{44}) \frac{\partial^2 \bar{w}}{\partial x \partial z} - \bar{p}_{,x} + \omega^2 \rho_f \bar{u} + \omega^2 \rho_f F(\omega^2 \rho_f \bar{u} - \bar{p}_{,x}) = 0 \\ (C_{12} + C_{66}) \frac{\partial^2 \bar{u}}{\partial x \partial y} + (C_{66} \frac{\partial^2}{\partial x^2} + C_{11} \frac{\partial^2}{\partial y^2} + C_{44} \frac{\partial^2}{\partial z^2}) \bar{v} + \\ (C_{13} + C_{44}) \frac{\partial^2 \bar{w}}{\partial y \partial z} - \bar{p}_{,y} + \omega^2 \rho_f \bar{v} + \omega^2 \rho_f F(\omega^2 \rho_f \bar{v} - \bar{p}_{,y}) = 0 \\ (C_{13} + C_{44}) \frac{\partial^2 \bar{u}}{\partial y \partial z} + (C_{44} \frac{\partial^2}{\partial x^2} + C_{44} \frac{\partial^2}{\partial y^2} + C_{33} \frac{\partial^2}{\partial z^2}) \bar{w} + \\ C_{44} + C_{13}) \frac{\partial^2 \bar{w}}{\partial x \partial z} - \bar{p}_{,z} + \omega^2 \rho_f \bar{w} + \omega^2 \rho_f F(\omega^2 \rho_f \bar{w} - \bar{p}_{,z}) = 0 \end{cases} \quad (8)$$

Similarly, Fourier transformation with respect to time is performed on Eq. (2). Then by substituting the results obtained into Eq. (7), the balance equation of fluid in frequency domain is expressed as:

$$(F\omega^2 \rho_f K_d + K_d) \left( \frac{\partial \bar{u}}{\partial x} + \frac{\partial \bar{v}}{\partial y} + \frac{\partial \bar{w}}{\partial z} \right) + n\bar{p} - FK_d \left( \frac{\partial^2}{\partial x^2} + \frac{\partial^2}{\partial y^2} + \frac{\partial^2}{\partial z^2} \right) \bar{p} = 0 \quad (9)$$

Stress boundary conditions and flow boundary condition in frequency domain of the FEM model are given as:

$$\begin{cases} \sigma_x l + \tau_{xy} m + \tau_{xz} n = f_x \\ \tau_{yx} l + \sigma_y m + \tau_{yz} n = f_y \\ \tau_{zx} l + \tau_{zy} n + \sigma_z m = f_z \end{cases} \quad (10)$$

$$\bar{q} = \rho_f g \bar{v}_n = -K_d \left( \frac{\partial}{\partial x} l + \frac{\partial}{\partial y} m + \frac{\partial}{\partial z} n \right) \bar{p} \quad (11)$$

where  $f_i$  ( $i = x, y, z$ ) are components of external forces in  $x, y, z$  directions;  $l, m, n$  are directions cosine, respectively;  $\bar{q}$  is the flow of pore water;  $\bar{v}_n$  is flow velocity of pore water.

Combining the constitutive equation and applying the Galerkin method to Eqs. (8)–(11), and then incorporating the developed shape function and performing wave-number expansion on the resulting equation in  $x$ -direction, the 2.5D FEM governing equations in wave-number domain and frequency domain can be derived by conventional finite element method, which are given by:

$$(\mathbf{K}_{up} - \mathbf{M}_{up}) \bar{\mathbf{u}} + (\mathbf{Q}'_{up} - \mathbf{Q}_{up}) \bar{\mathbf{p}} = \bar{\mathbf{f}}_{up}^s \quad (12a)$$

$$(\mathbf{H}_{up} + \mathbf{S}_{up}) \bar{\mathbf{p}} + \mathbf{Q}''_{up} \bar{\mathbf{u}} = \bar{\mathbf{f}}_{up}^q \quad (12b)$$

where  $\mathbf{K}_{up}$  is stiffness matrix;  $\mathbf{M}_{up}$  is mass matrix;  $\mathbf{Q}'_{up}$ ,  $\mathbf{Q}''_{up}$  and  $\mathbf{Q}_{up}$  are solid and fluid coupling matrixes;  $\mathbf{H}_{up}$  and  $\mathbf{S}_{up}$  are Jacobian matrixes;  $\bar{\mathbf{f}}_{up}^s$  and  $\bar{\mathbf{f}}_{up}^q$  are equivalent node load vectors;  $\bar{\mathbf{u}}$  is node displacement matrix; variables with '–' above indicate the component in wave-number domain.

Artificial boundary has a non-negligible influence on the calculation accuracy. Referring to Gao et al. [11], this paper adopted a 2.5D viscoelastic dynamic artificial boundary to model the wave propagation in

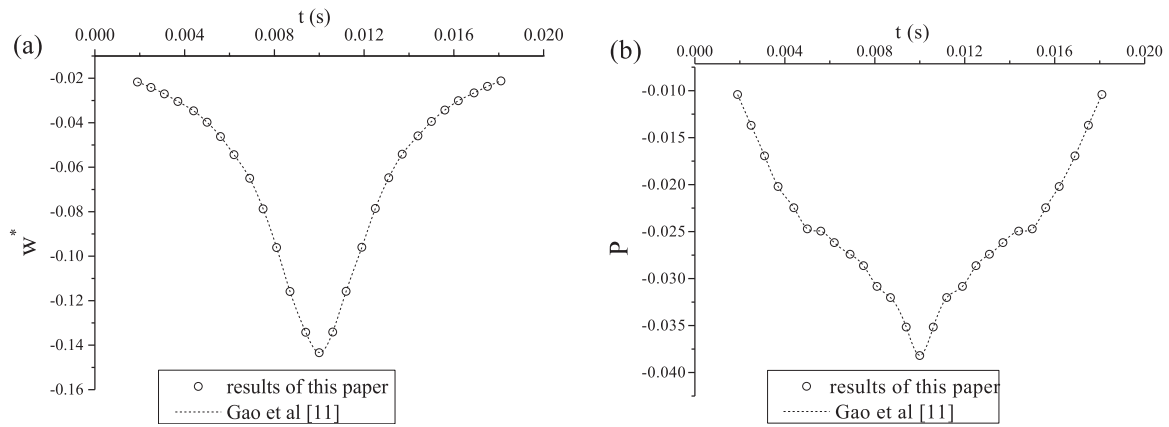


Fig. 1. Verification of the 2.5 D FEM: (a) Normalized displacement time history curve; (b) Normalized pore pressure time history curve.

Table 1

Calculation parameters of transversely isotropic saturated soil.

Parameters	Values
Density $\rho$ (kg/m <sup>3</sup> )	1800
Horizontal elastic modulus $E_{hh}$ (MPa)	5.46
Vertical elastic modulus $E_{vh}$ (MPa)	7.86
Vertical shear modulus $G_v$ (MPa)	2.45
Horizontal Poisson ratio $\mu_{hh}$	0.35
Vertical Poisson ratio $\mu_{vh}$	0.34
Material damping $\beta$	0.05
Bulk elastic modulus of fluid $K_f$ (MPa)	$2 \times 10^3$
Dynamic permeability coefficient $K_d$ (m/s)	$2 \times 10^{-7}$
Porosity $n$	0.54

far-field of transversely isotropic saturated ground. And drainage boundary is set on the surface of this model.

### 3. Numerical examples and discussions

In order to verify the validity and reliability of the proposed method in analysis of the vibration of transversely isotropic saturated soils, numerical results obtained from this paper are degenerated to compare with Gao's results [11] by setting that  $E_{hh} = E_{hv}$ ,  $\mu_{hh} = \mu_{vh}$ ,  $G_v = E_{hh}/2(1 + \nu_{hh})$ . Velocity of the moving loads acting on the ground surface is  $0.5V_s$  ( $V_s = \sqrt{G/\rho}$  is the shear wave velocity of soil). The dynamic responses at 1.0 m beneath the ground surface were investigated. Fig. 1 shows the normalized vertical displacement  $w^* = wG/F_{max}$  and excess pore water pressure  $P = p/F_{max}$  predicted by current model and that of Gao et al. [11], where  $F_{max}$  and  $G$  are the train wheel load and soil shear modulus, respectively. It is observed from

Fig. 1 that these two results agree with each other, which demonstrates the accuracy of the suggested model.

#### 3.1. Parameters of calculation model

The track is a 32 m standard rail normally used in Beijing-Shanghai high-speed railway. Its bending rigidity is  $EI = 38.0496$  kN m, and the comprehensive quality is 401 kg/m. The adopted high-speed train model is the CRH5, which is similar to the model in Bian et al. [12]. There are 8 carriages composing one unit, including 2 motor cars and 6 trailers. The length of train is 205.2 m, including 16 wheel sets in total. Length of trailer is 25 m, length of motor car is 27.6 m, distance of bogie center is 17.5 m, fixed wheelbase is 2.7 m, and average axle load is 17 t. The soil parameters are shown in Table 1. The train velocity is 200 km/h, corresponding to the high-speed train moving near the downtown.

#### 3.2. Effects of horizontal and vertical elastic moduli

In order to discuss the effects of horizontal elastic modulus, vertical elastic modulus was taken as a constant of 7.86 MPa; horizontal elastic moduli were adopted as 9.06 MPa, 7.86 MPa, 6.66 MPa and 5.46 MPa, respectively. Other soil parameters are identical to that in Table 1 (similarly hereinafter). Fig. 2 presents the amplitude of vertical displacement along the distance from the track center for different horizontal elastic modulus and distribution of excess pore water pressure along the depth beneath the track center. It can be observed from Fig. 2(a) that ground vibration amplitudes decrease with the increase of horizontal elastic modulus. This is attribute from that, the increment of the horizontal modulus exerts an overall confining action on the soil,

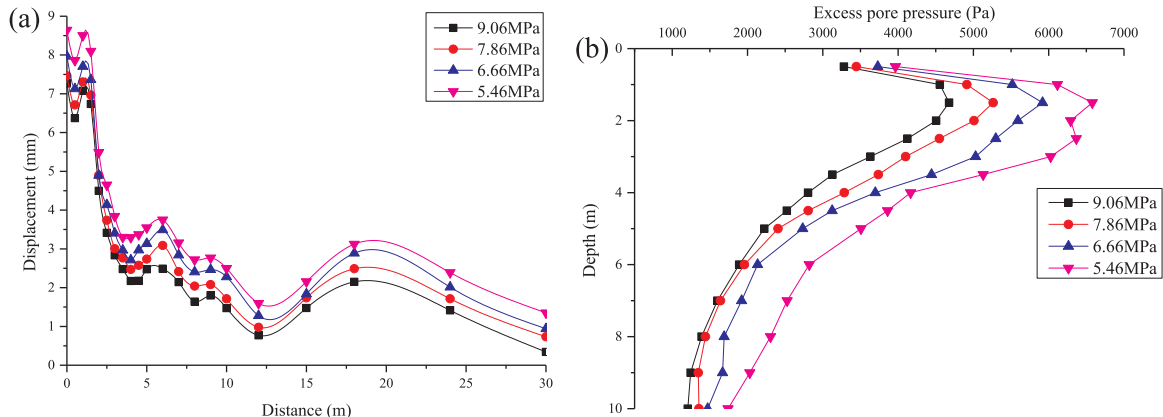


Fig. 2. Effects of horizontal elastic modulus: (a) Attenuation of peak amplitude along ground surface; (b) Distribution of excess pore water pressure along depth.

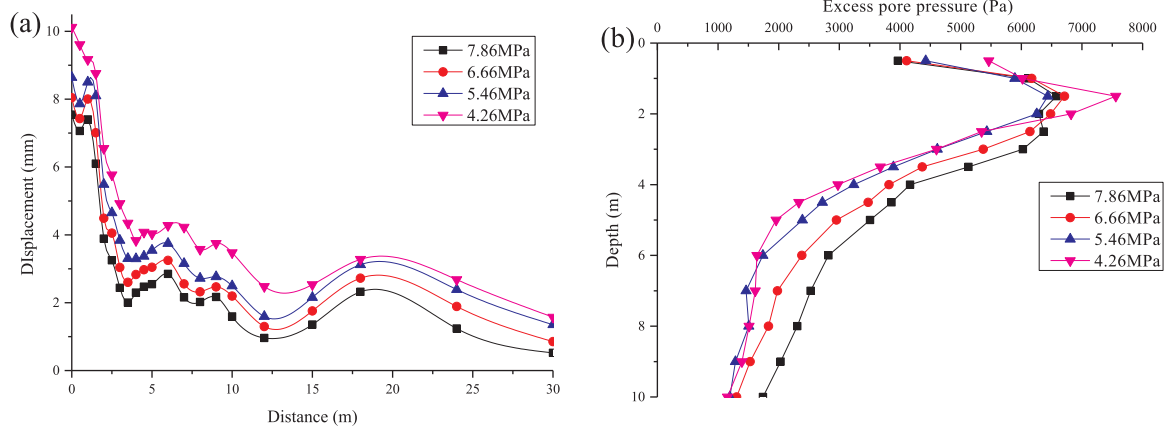


Fig. 3. Effects of vertical elastic modulus: (a) Attenuation of peak amplitude along ground surface; (b) Distribution of excess pore water pressure along depth.

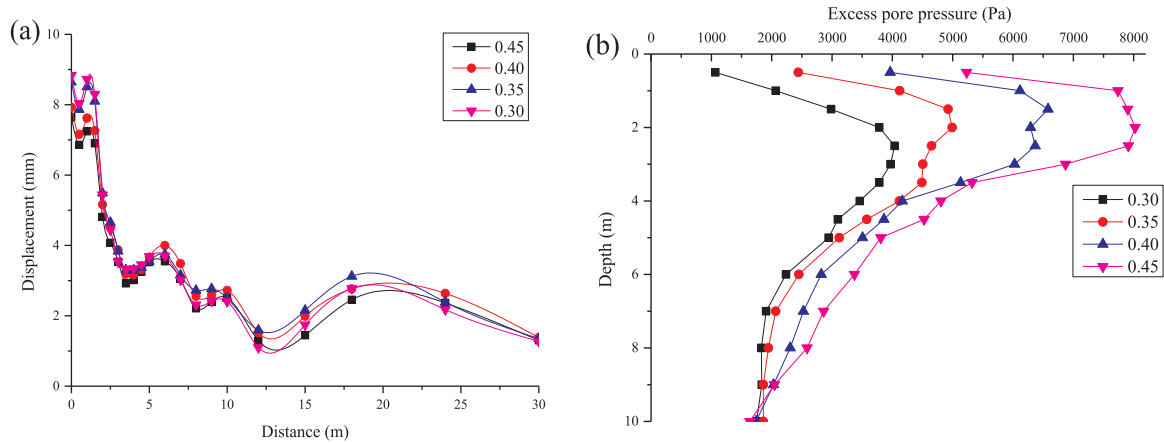


Fig. 4. Effects of horizontal Poisson ratio: (a) Attenuation of peak amplitude along ground surface; (b) Distribution of excess pore water pressure along depth.

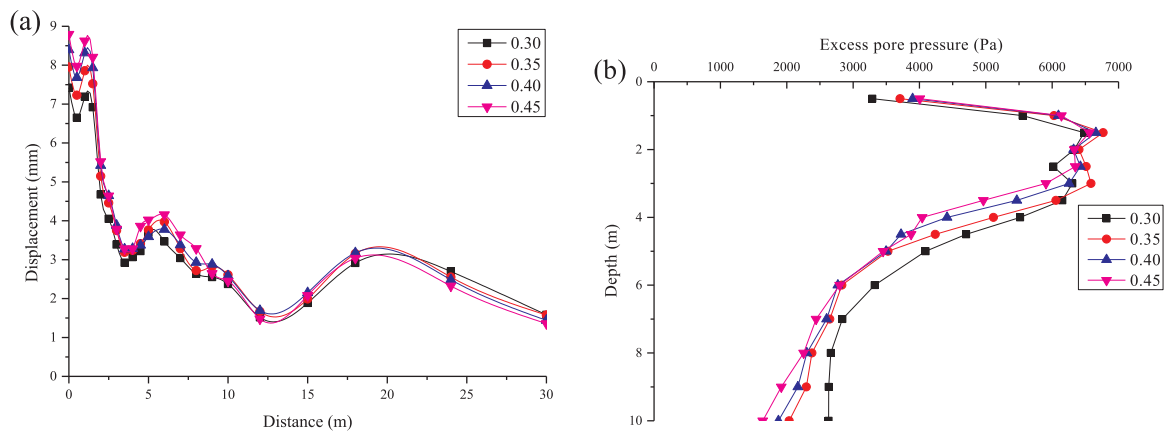


Fig. 5. Effects of vertical Poisson ratio: (a) Attenuation of peak amplitude along ground surface; (b) Distribution of excess pore water pressure along depth.

thus make the vertical displacement more difficult to happen. Maximum excess pore water pressures occur at 2 m beneath ground surface, as shown in Fig. 2(b). The excess pore water pressures increase with the decrease of horizontal elastic modulus. The soil becomes isotropic when  $E_{hh} = E_{hv}$ ,  $\mu_{hh} = \mu_{vh}$ ,  $G_v = E_{hh}/2(1 + \nu_{hh})$ .

To investigate the effects of vertical elastic modulus, horizontal elastic modulus was taken as a constant of 5.46 MPa, and vertical elastic moduli were set as 7.86 MPa, 6.66 MPa, 5.46 MPa and 4.26 MPa, respectively. Fig. 3(a) shows that the vibration amplitude decreases with the increase of vertical modulus and the vibration attenuates significantly within 5 m from the center of track. Vertical

elastic modulus has a greater influence than horizontal elastic modulus compared to Fig. 2(a). Excess pore water pressures decrease with the increase of vertical elastic modulus, as presented in Fig. 3(b). By comparing Figs. 2(b) and 3(b), it is concluded that with the increase of horizontal elastic modulus, deformation of soil and excess pore water pressure decrease; while with the increase of vertical elastic modulus, excess pore water pressures near ground surface decrease, and that in the deeper soils increase. This indicates that horizontal and vertical elastic modulus exerts different effects on excess pore water pressures.

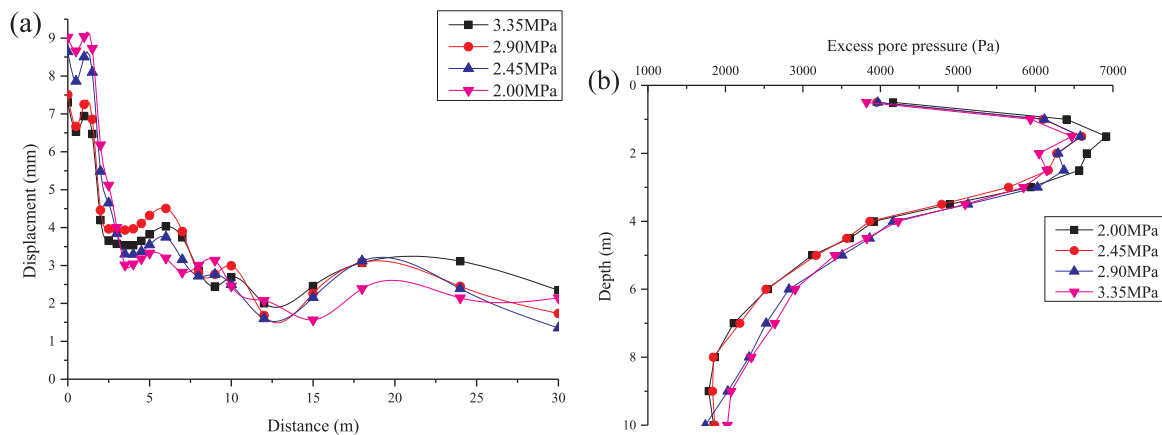


Fig. 6. Effects of shear modulus: (a) Attenuation of peak amplitude along ground surface; (b) Distribution of excess pore water pressure along depth.

### 3.3. Effects of horizontal and vertical Poisson ratio

To study the effects of horizontal Poisson ratio, vertical Poisson ratio was taken as a constant of 0.32, and horizontal Poisson ratios were respectively adopted as 0.30, 0.35, 0.40 and 0.45. The results in Fig. 4(a) indicate that the effects of Poisson ratio on ground vibrations are less obvious than those of the elastic modulus. Fig. 4(b) shows the excess pore water pressures for different horizontal Poisson ratios, which indicates that excess pore water pressure generally increases with the increase of horizontal Poisson ratio.

Effects of vertical Poisson ratio is covered by setting horizontal Poisson ratio as a fixed value of 0.32, and vertical Poisson ratios were adopted as 0.30, 0.35, 0.40, and 0.45, respectively. Fig. 5(a) shows the attenuation curves of vibration displacement for different vertical Poisson ratios, which indicates that displacement amplitude increases with the increase of vertical Poisson ratio near the center of track, and the attenuation is different from that shown in Fig. 4(a). Fig. 5(b) shows the excess pore water pressures for different vertical Poisson ratios. It is observed that the influence of vertical Poisson ratio to excess pore water pressure is less significant compared to horizontal Poisson ratio.

### 3.4. Effects of shear modulus

In this section, the horizontal shear modulus of transversely isotropic soil is the same to that of isotropic soil, while vertical shear modulus is an independent variable. Fig. 6(a) shows the attenuation curves of vibration displacement for different shear moduli (2.0 MPa, 2.45 MPa, 2.90 MPa, 3.35 MPa). It is observed from Fig. 6(a) that the amplitudes of ground vibrations decrease with the increase of shear modulus. Fig. 6(b) shows the excess pore water pressure curves for different shear modulus. It can be seen from Fig. 6(b) that, excess pore water pressure increases with the decrease of shear modulus in the depth of 3 m, and the maximum excess pore water pressure occurs at 2 m beneath track center for different shear moduli.

## 4. Conclusions

In this paper, numerical simulations of ground vibrations in transversely isotropic saturated medium induced by high-speed trains were performed. The displacement-pore pressure ( $u$ - $p$ ) format 2.5D FEM model and dynamic viscoelastic boundary condition in transversely isotropic medium were presented. The proposed numerical method was

validated by a published example in the literature. Effects of horizontal and vertical elastic modulus, horizontal and vertical Poisson ratio and shear modulus on vertical ground vibration and excess pore water pressure were analyzed under high-speed train loads, respectively. The numerical results show that the decrement of vibration amplitude and excess pore water pressure caused by increment of vertical elastic modulus is larger than that caused by horizontal elastic modulus. Both horizontal and vertical Poisson ratios have little effects on ground vibrations, whereas the horizontal Poisson ratio increment results in a great increase on excess pore water pressure.

## Acknowledgments

The project was supported by the National Natural Science Foundation of China (No. 41772288).

## References

- [1] Kuwano R, Wicaksono RI, Mulmi S. Small strain stiffness of coarse granular materials measured by wave propagation. In: Proceedings of 4th international symposium on deformation characteristics of geomaterials. IS-Atlanta; 2008. p. 749–56.
- [2] Nishimura S. Cross-anisotropic deformation characteristics of natural sedimentary clays. *Geotechnique* 2014;64(12):981–96.
- [3] Papargyri-Beskou S, Polyzos D, Beskos DE. Wave dispersion in gradient elastic solids and structures: a unified treatment. *Int J Solids Struct* 2009;46(21):3751–9.
- [4] Zymnis DM, Chatzigiannellis I, Whittle AJ. Effect of anisotropy in ground movements caused by tunnelling. *Geotechnique* 2013;63(13):1083–102.
- [5] Ahmadi SF, Eskandari M. Vibration analysis of a rigid circular disk embedded in a transversely isotropic solid. *J Eng Mech Div ASCE* 2013;140(7):04014048.
- [6] Ogden RW, Singh B. The effect of rotation and initial stress on the propagation of waves in a transversely isotropic elastic solid. *Wave Motion* 2014;51(7):1108–26.
- [7] Ai ZY, Ren GP. Dynamic analysis of a transversely isotropic multilayered half-plane subjected to a moving load. *Soil Dyn Earthq Eng* 2016;83:162–6.
- [8] Abedrahim H. Coupling of finite and hierarchical infinite elements: application to a non-homogeneous cross-anisotropic half-space subjected to a non-uniform circular loading. *Int J Numer Analyses Methods Geomech* 2012;37:1552–73.
- [9] Yang YB, Hung HH. A 2.5 D finite/infinite element approach for modelling viscoelastic bodies subjected to moving loads. *Int J Numer Methods Eng* 2001;51(11):1317–36.
- [10] Yang YB, Huang HH, Chang DW. Train-induced wave propagation in layered soils using finite/infinite element simulation. *Soil Dyn Earthq Eng* 2003;23(4):263–78.
- [11] Gao GY, Chen QS, He JF, Liu F. Investigation of ground vibration due to trains moving on saturated multi-layered ground by 2.5D finite element method. *Soil Dyn Earthq Eng* 2012;40:87–98.
- [12] Bian X, Jiang H, Chang C, et al. Track and ground vibrations generated by high-speed train running on ballastless railway with excitation of vertical track irregularities. *Soil Dyn Earthq Eng* 2015;76:29–43.